Locking and Arnold tongues in an infinite-dimensional system: The nuclear magnetic resonance laser with delayed feedback

J. Simonet, M. Warden,* and E. Brun
Physics Institute, University of Zürich, Zürich, Switzerland
(Received 13 June 1994)

Experimental observations and computer simulations of locked states in an infinite-dimensional periodically Q modulated NMR laser with feedback are presented. Arnold tongues (AT's) were observed both for a harmonic and an anharmonic (square-wave) modulation. The width of selected AT's were significantly larger for the anharmonic modulation than for the harmonic modulation. In addition, the AT's were observed to split into regimes of locking to different fundamental limit cycles as the modulation amplitude was increased. Significant deviations of the locking behavior from predictions of the one-dimensional circle map were observed. The experimental results agreed in an excellent way with simulations with a phenomenological Bloch-Kirchhoff model with a heuristic relaxation term and consequently present an exemplary test for the model.

PACS number(s): 05.45.+b, 76.60.−k

I. INTRODUCTION

Various nonlinear dissipative solid-state systems exhibit temporal mode-locking phenomena. These include charge density wave systems [1] driven by radio frequency electric fields, resistively shunted Josephson junctions driven by microwave fields [2], power modulated spin wave systems [3], barium sodium niobate single crystals driven by ac currents [4], and a NMR laser with injected signal [5,6].

The NMR laser is ideal for the study of locking phenomena because of its excellent long-term stability and large signal-to-noise ratio. The NMR laser without feedback has been studied intensively, and the dynamics have been analyzed both in the regular and chaotic regimes. In addition, the system has been very well modeled by the Bloch-Kirchhoff equations with phenomenological damping terms [7,8]. Here locking phenomena are reported for the ruby nuclear magnetic resonance (NMR) laser with delayed feedback and quality factor (Q) modulation [9]. Laser systems with delayed feedback but without Q-factor modulation have been studied extensively [10]. In addition to the locking phenomena caused by a harmonic modulation, the influence of a square-wave modulation was observed. The parameters of the NMR laser without Q modulation were tuned so that the system evolved to a limit cycle of fundamental frequency $\omega_0=\omega_0(\tau,\epsilon)$, where τ is the delay time of the feedback signal and ϵ is the feedback signal amplitude. Under these conditions locking was observed at various rational frequency ratios $\omega_m/\omega_0'=p/q=1/5,1/4,\ldots,1/1,\ldots,2/1$, where p and q are integers, ω_m is the modulation frequency, and $\omega_0'=\omega_0+\Delta\omega_0(V_{m0},\omega_m)$ is the frequency of the laser output which deviated from ω_0 by an amount $\Delta\omega_0$ depending on the modulation amplitude V_{m0} and the modulation frequency ω_m. The particular limit cycle studied was anharmonic and, in contrast to the sinusoidal case, the square-wave modulation caused a significant increase in $\Delta\omega_0$ for small modulation amplitudes V_{m0}. For larger amplitudes, however, the locking was suppressed for the square-wave modulation. In addition, the Arnold tongues broke up into well defined regimes, which could be identified as corresponding to different oscillation modes of the laser, set up by the Q modulation.

II. EXPERIMENTAL SETUP

The experimental setup is shown in Fig. 1. The ruby NMR-laser activity was produced by the nuclear spins of the ^{27}Al ($I=5/2$) in the single crystal ruby $Al_2O_3:Cr^{+3}$. The crystal was subjected to a static external magnetic field of $B_0\approx 1.1$ T, where the Zeeman splitting and quadrupole interaction resulted in five possible NMR spin-flip transitions $\Delta m=\pm 1$. The ruby crystal was placed within a coil of induction L which was part of a narrow band laser-cavity (LC) circuit with frequency $\omega_c=(1/LC)^{1/2}$. The LC circuit was tuned to the strong central $(-\frac{1}{2},+\frac{1}{2})$ spin-flip transition frequency $\omega_a=gB_0$, thus enforcing single-mode activity and allowing the system to be described by a fictitious two-level spin-$\frac{1}{2}$ system. The spin population inversion was obtained by means of dynamical nuclear polarization (DNP) [11] where the electron spins of the Cr^{3+} were pumped with microwaves slightly above resonance at about 30.2 GHz and the electron-nuclear spin interaction caused the Zeeman energy of the Cr^{3+} electron spin system to be transferred to the ^{27}Al nuclear spins [5].

In the experiments described here the laser output, which was monitored as the voltage V_{out} between the two capacitors C_1 and C_2 of the capacitive voltage splitter, was demodulated, amplified, and then fed back to a

*Corresponding author. FAX: (+41) 1 257-5704. Electronic address: warden@physik.unizh.ch

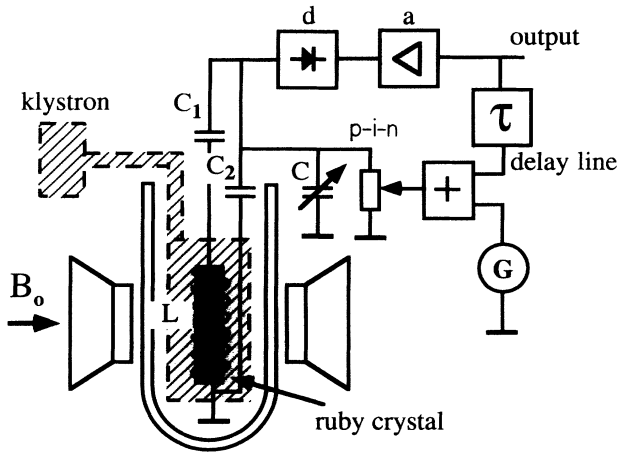

FIG. 1. Schematic representation of the experimental setup for the ruby NMR laser with delayed feedback and quality factor modulation. The gain medium consisted of the nuclear spins of the ^{27}Al nuclei within a ruby crystal which was subjected to a static field B_0. Population inversion was obtained by dynamic nuclear polarization with microwaves supplied by a klystron. The resonator was composed of a coil, a capacitive voltage splitter (C_1,C_2) and a tuning capacitor C, and a variable resistor (*p-i-n* diode). The laser output was fed back to the *p-i-n* diode after a delay time τ. In order to observe locking phenomena, periodic voltage modulation (G) was applied to the *p-i-n* diode.

voltage-controlled resistor (*p-i-n*-diode) after a delay time τ. The change in resistance resulted in a change of the quality factor Q of the resonator. In order to observe locking, an additional periodic voltage modulation $V_m(t)$ was added to the feedback signal. Either a harmonic modulation $V_m(t)=V_{m0}\sin(\omega_m t)$ or a square-wave modulation $V_m(t)=V_{m0}\mathrm{sgn}[\sin(\omega_m t)]$ was employed.

III. EXTENDED BLOCH EQUATIONS WITH DELAY

The experiments were very well described by the extended Bloch laser (EBL) model [7]. Under the conditions of single-mode operation and zero detuning from the central spin-flip transition, the rotating frame approximation is valid and the EBL equations are given by

$$\begin{aligned}\frac{dB_u}{dt}&=-\frac{\omega_c}{2Q(t)}B_u-\chi M_v\ ,\\ \frac{dM_v}{dt}&=-\gamma_\perp M_v\left[1+\frac{\alpha}{3}|M_v|\right]+9gM_zB_u\ ,\\ \frac{dM_z}{dt}&=-\gamma_\parallel(M_z-M_e)-gM_vB_u\ ,\end{aligned}\tag{1}$$

where M_v and M_z are the transverse and longitudinal components of the nuclear magnetization which arises from the active ^{27}Al spins, B_u is the transverse component of the radiation magnetic field, $g=6.97\times10^7$ $(\mathrm{T\,s})^{-1}$ is the gyromagnetic ratio of the ^{27}Al spins, $\gamma_\perp$ is the decay rate of the transverse magnetization, $\gamma_\parallel$ is the DNP pump rate, M_e is an effective pump magnetization assigned to the DNP-pump system, χ is the coupling constant, and ω_c is the laser frequency. It is well known that the phenomenological Bloch equations often provide incorrect predictions in solids [11]. Therefore, we replaced $\gamma_\perp$ by $\gamma_\perp[1+(\alpha/3)|M|_v]$, thus taking into account lowest-order nonexponential dephasing which is proportional to the amplitude M_v of the transverse nuclear magnetization. Assuming the lowest-order nonexponential dephasing term to be proportional to the absolute value of M_v guarantees a symmetrical deviation from linearity similar to the case of a strong spring.

The time dependent quality factor $Q(t)$ was given by $Q(t)=Q_0-pV_{p\text{-}i\text{-}n}(t)$, where Q_0 was the unperturbed quality factor obtained with a fixed bias voltage applied to the *p-i-n* diode, $V_{p\text{-}i\text{-}n}$ was the feedback plus modulation voltage applied to the *p-i-n* diode, and $p=23.5\ \mathrm{V}^{-1}$ was a factor given by the characteristics of the *p-i-n* diode, which was determined experimentally. With delayed feedback and modulation, the additional voltage applied to the *p-i-n* diode was

$$V_{p\text{-}i\text{-}n}(t)=V_{m0}\sin\omega_m t+\zeta Q(t-\tau)|M_v(t-\tau)|\ ,\tag{2}$$

where $\zeta=\delta\mu_0\eta AN\omega_c$ was given by Faraday's law of induction, and δ represented a variable factor containing the capacitive voltage divider, an amplification factor, and the characteristics of the demodulator. Finally, τ was the delay time. A relative quality factor $q(t)$ was introduced in the following way:

$$q(t)=\frac{Q(t)}{Q_0}=1-v_{m0}\sin\omega_m t-\epsilon q(t-\tau)|M_v(t-\tau)|\ ,\tag{3}$$

where $v_{m0}=pV_{m0}/Q_0$, and the feedback coupling was $\epsilon=p\zeta$.

The output of the experiment was given by

$$V_{\mathrm{out}}=\delta\mu_0NA\eta\omega_cQ|M_v|\ ,\tag{4}$$

where μ_0 was the permeability of free space, N was the number of turns of the NMR coil, A was the cross section of the NMR coil, and η was the filling factor of the NMR coil.

In order to obtain improved numerical accuracy, the EBL model was expressed in the dimensionless time $t'=t\gamma_\perp$ and dimensionless variables

$$\begin{aligned}&x=\frac{3g}{\gamma_\perp}B_u\ ,\quad y=-\frac{6g\chi Q_0}{\omega_c\gamma_\perp}M_v\ ,\\ &\text{and } z=\frac{18g\chi Q_0}{\omega_c\gamma_\perp}(M_z-M_e)\ ,\end{aligned}\tag{5}$$

resulting in

$$\begin{aligned}\frac{dx}{dt'}&=\sigma\left[y-\frac{x}{q'(t')}\right]\ ,\\ \frac{dy}{dt'}&=-y(1+ay)+rx-xz\ ,\\ \frac{dz}{dt'}&=-bz+xy\ .\end{aligned}\tag{6}$$

The parameters are

$$\sigma=\frac{\omega_c}{2Q_0\gamma_\perp}\ ,\quad r=\frac{18g\chi Q_0}{\omega_c\gamma_\perp}M_e\ ,$$
$$a=\frac{\alpha\omega_c\gamma_\perp}{18g\chi Q_0},\ \text{and}\ b=\frac{\gamma_\parallel}{\gamma_\perp}\ . \tag{7}$$

The variation of the relative quality factor is now given by

$$q'(t')=1-v_{m0}\sin(\omega'_m t')-\epsilon' q'(t'-\tau')y(t'-\tau')\ , \tag{8}$$

where $\tau'=\tau\gamma_\perp$ is the delay time, $\omega'_m=\omega_m/\gamma_\perp$ the modulation frequency, and $\epsilon'=\epsilon\omega_c\gamma_\perp/6g\chi Q_0$, all expressed in dimensionless units. Finally, by introducing the rescaled variables

$$X=x/x_0\ ,\quad Y=y/x_0\ ,\ \text{and}\ Z=(z-z_0)/x_0\ , \tag{9}$$

with $x_0=\pm\sqrt{b(r-1)}$, and setting $t''=t'x_0$, Eqs. (6) were transformed to

$$\frac{dX}{dt''}=\sigma'\left[Y-\frac{X}{q''(t'')}\right],$$
$$\frac{dY}{dt''}=-Y(c+aY)+X(c-Z)\ , \tag{10}$$
$$\frac{dZ}{dt''}=-\beta Z-1+XY\ ,$$

where $\sigma'=\sigma/x_0\approx 384$, $c=1/x_0\approx 79$, and $\beta=b/x_0\approx 1.57\times10^{-2}$. Since the damping rate of X is $\sigma'\gg c,\beta$, the variable X can be adiabatically eliminated [12] by setting, to lowest order, $dX/dt''=0$, leading to

$$\frac{dY}{dt''}=-Y[(c+aY)+q''(t'')(Z-c)]\ ,$$
$$\frac{dZ}{dt''}=-\beta Z-1+q''(t'')Y^2\ , \tag{11}$$

where

$$q''(t'')=1-v_{m0}\sin(\omega''t'')-\epsilon'' q''(t''-\tau'')Y(t''-\tau'')$$

with $\epsilon''=x_0\epsilon'$, $\tau''=x_0\tau'$, and $\omega''_m=x_0/\omega'_m$. For a compilation of the NMR-laser parameters, see Table I.

TABLE I. Experimentally determined NMR-laser parameters for standard running conditions. The numerical values are used to calculate the system parameters of the EBL model.

NMR-laser parameters		
gyromagnetic ratio	g	6.97×10^7 1/s T
quality factor	Q_0	310
static NMR field	B_0	1.109 T
laser frequency	ν_c	12.3×10^6 [Hz]
pump magnetization	M_e	−0.75 [A/m]
longitudinal pump rate	$\gamma_\parallel$	4.76 [1/s]
transverse decay rate	$\gamma_\perp$	2.38×10^4 [1/s]
EBL dephasing coefficient	α	0.607 [m/A]
filling factor	η	0.42
coupling constant	χ	10.19 [Tm/As]
Number of windings	N	30
cross section of the NMR coil	A	47.746×10^{-6} [m^2]

Equations (11) were used for the simulations presented below. Because of the presence of the delayed feedback, this model represents an infinite-dimensional system. However, the fractal dimensions determined by the method described in [13,14] yield values between 2 and 3, as noted earlier [9]. Such a reduction in effective dimension has been shown to prevail in infinite-dimensional systems [15]. Figure 2 shows the numerically determined bifurcation diagrams as a function of the feedback coupling constant ϵ for the EBL model with feedback but without modulation ($V_{m0}=0$). In Fig. 2(a) the delay time was $\tau=105$ ms. For each ϵ value, the first 50 maxima were plotted after a transient time of 5 s. For small feedback coupling $\epsilon<0.11$ the system was in a steady state; at about $\epsilon\approx0.11$ a bifurcation occurred to a period-1 limit cycle, which increased in magnitude until at $\epsilon\approx0.15$ a further bifurcation to a quasiperiodic state took place, which again was followed by a period-1 limit cycle at $\epsilon\approx0.20$. The locking experiments were performed at $\epsilon=0.25$, where the system evolved to a period-1 limit cycle of fundamental frequency $\nu_0=41.65$ Hz. This operating point is indicated by a dashed line in Fig. 2. For comparison, the bifurcation diagram is also shown for a smaller delay time of $\tau=41$ ms [Fig. 2(b)]. Here the value of $\epsilon=0.25$ lies inside the quasiperiodic regime.

Figure 3 shows the regions of various stable periodic orbits in the parameter space given by the feedback coupling ϵ vs the delay time τ. The following color coding was used: a time series of fixed length (≈1 s) was calculated for each value of τ and ϵ. Then all maxima of the time series were determined. The color was given according to the number of different values taken by the maxima. When no maxima were present (constant signal), the

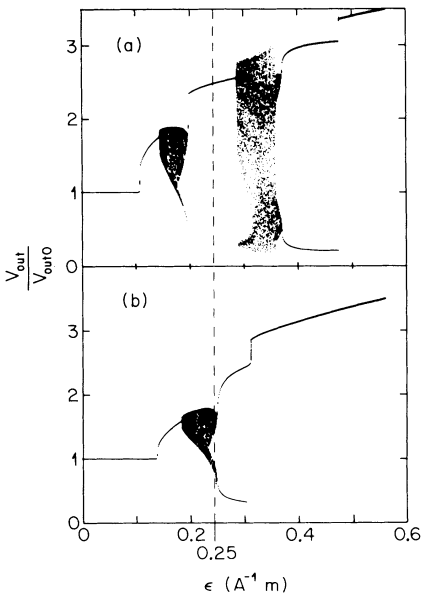

FIG. 2. Numerically determined bifurcation diagrams. For each feedback value ϵ the first 50 maxima were plotted after a transient time of 5 s. (a) $\tau=105$ ms, (b) $\tau=41$ ms. The dashed line corresponds to the ϵ value of the limit cycle used in subsequent studies of locking phenomena.

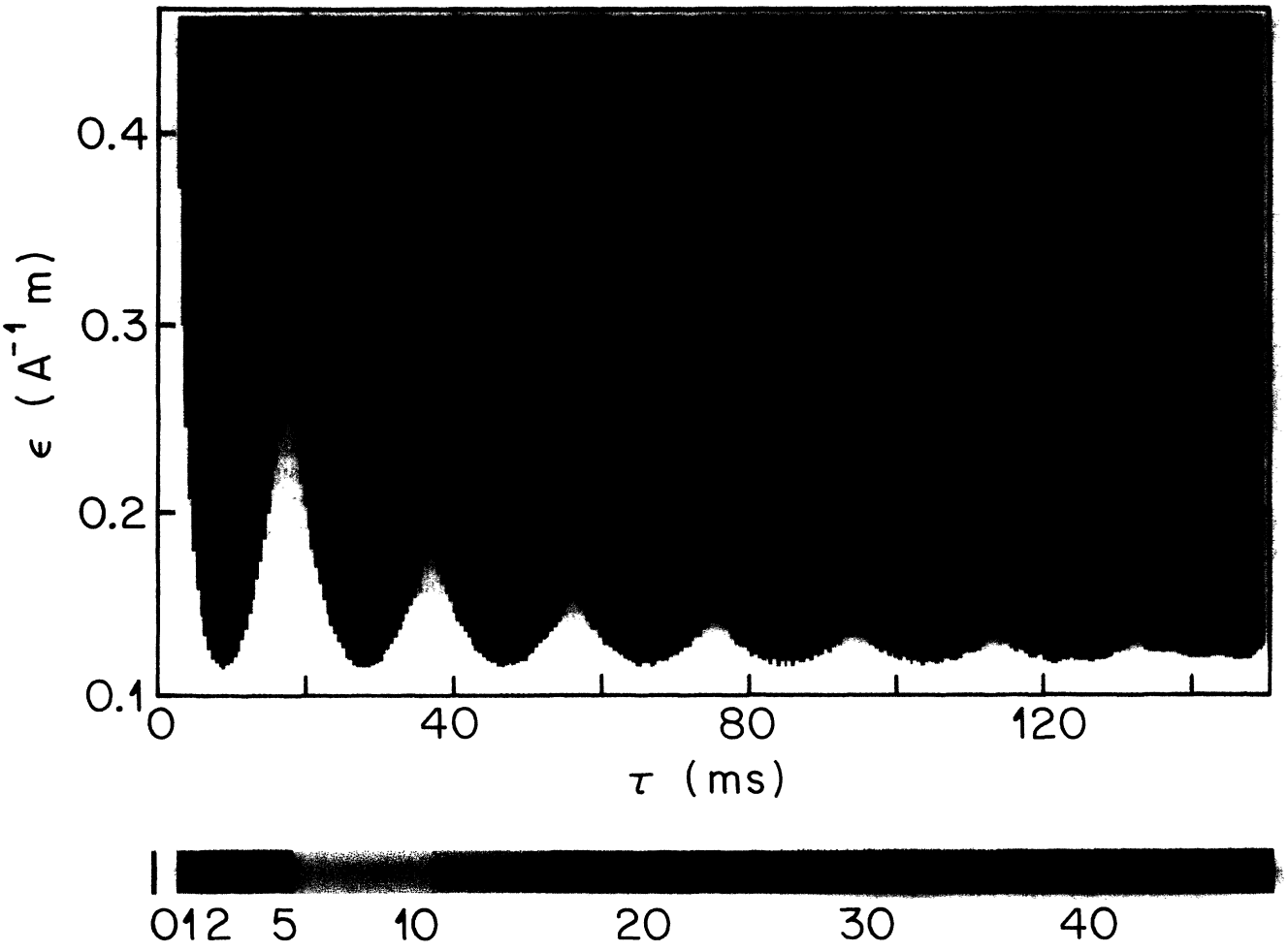

FIG. 3. Computed asymptotic properties of the solutions of the EBL model in the parameter space of delay time τ vs feedback coupling ϵ. The color coding corresponds to the number of maxima of different values in a time series of given length. White, stationary solutions. Light blue, period-2 solutions. Bottom, index showing the color used for a particular number of different maxima.

point was colored white. This case corresponded to stationary solutions. When all maxima had the same value this corresponded to a periodic behavior, and the point was colored light blue. The correspondence between color coding and the number of different maxima values is shown at the bottom of Fig. 3. The fractal dimensions were estimated from selected time series within the red and black regions, revealing values up to 3. Experimentally this behavior was reproduced in an excellent way for a selected region of the parameter space. The bifurcation diagrams shown in Fig. 2 correspond to parameter variations along straight vertical lines at $\tau=105$ ms and at $\tau=41$ ms in Fig. 3.

IV. LOCKED STATES INDUCED BY HARMONIC MODULATION

Locked states were identified experimentally by plotting the laser output vs the modulation amplitude V_{m0}. When a stable Lissajous figure was found the system was considered to be locked. This procedure is demonstrated in Fig. 4, where the logarithm of the laser output is displayed vs the harmonic modulation $V_m = V_{m0}\sin(2\pi\nu_m t)$. Experimental results are shown on the left, and the corresponding numerical results, obtained from Eq. (11), are shown on the right. The frequency was $\nu_m \approx 70.3$ Hz and the amplitude $V_{m0}=0.09$ V. A stable Lissajous figure was observed which indicates that the laser was locked to half the modulation frequency. When the modulation frequency was lowered the system was no longer locked, resulting in a partial filling of the phase space.

The presence of more than one crossing point in Fig. 4 also indicates that the time dependence of the laser output was not harmonic. For a harmonic response the frequency ratios $1/n$ would result in a maximum of $n-1$ crossing points. The harmonic content of the free-running laser output signal is shown in Fig. 5 both for the experiment [Fig. 5(a)] and for the simulation [Fig. 5(b)]. The logarithm of the power spectral density was plotted as a function of the frequency. The power of the higher harmonics decayed roughly exponentially. The box

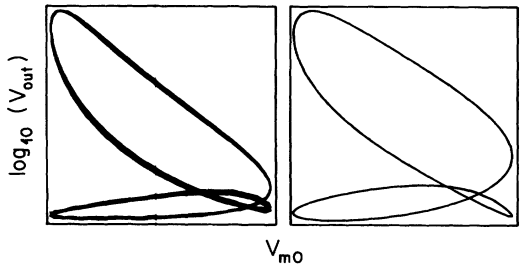

FIG. 4. Laser output $\log_{10}(V_{\text{out}})$ vs modulation signal. Left, experiment and right simulations using the EBL model [Eqs. (11)]. The modulation frequency ν_m was close to the frequency of the limit cycle, and the system was locked as evidenced by the closed Lissajous figures.

within Fig. 5(b) shows the logarithm of the power spectral density obtained from the laser output when the feedback strength was chosen slightly below the second bifurcation at $\epsilon=0.28$ [Fig. 2(a)]. A frequency appeared at $\nu_{00}\approx 34$ Hz which originated from an additional mode of the system. As shown below, this mode was manifest in the low frequency part of the 1/1 and 2/1 Arnold tongues (Fig. 6). The system was locked there to this fundamental frequency ω'_{00}.

The parameter space of (ω_m, V_{m0}) was scanned, and locked states were determined by two different methods. The results shown in Fig. 6 were obtained by using the procedure described above. The points correspond to parameter values where the system was locked. Several Arnold tongues could be identified. These include the rational ratios $\omega_m/\omega'_0=1/5$, 1/4, 1/3, 1/2, and 1/1. The gray areas in Fig. 6 are the locked states as determined from Eqs. (11). The simulated locked states were determined by the same procedure as the experimentally determined values, by calculating the time evolution of the

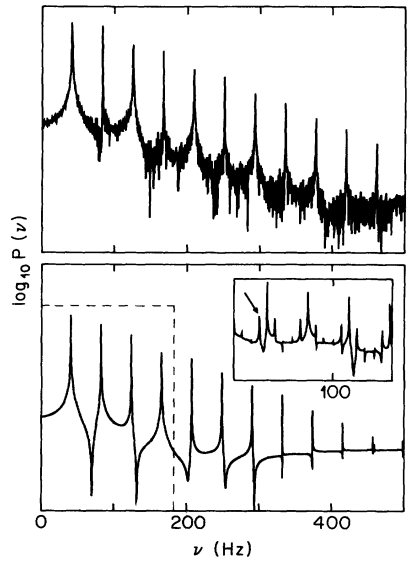

FIG. 5. Logarithm of the power spectral density vs frequency of the laser output without modulation for a feedback strength of $\epsilon=0.25$. Top, experiment and bottom, simulation. The inset (bottom) shows the spectrum for a value of the feedback strength $\epsilon=0.28$ which was chosen near the second bifurcation point (see Fig. 2). Note the appearance of a second frequency ν_{00} (arrow) below the fundamental frequency ν_0.

slowly varying laser output. After a transient of more than 100 periods of the modulation cycle, the output was plotted vs the modulation, and the stable Lissajous figures were identified. The results shown in Fig. 7 were obtained by performing a harmonic analysis of the time series, which were analyzed after a transient of approximately 100 periods of the modulation cycle. The following color coding was used: the highest Fourier peak

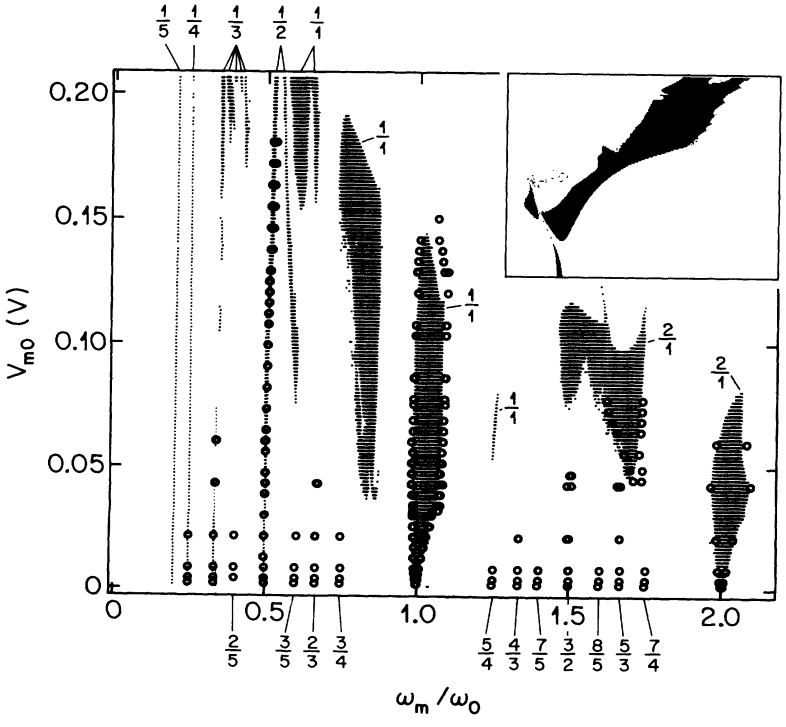

FIG. 6. Locked states in the parameter space of modulation frequency vs modulation amplitude. Circles, experiment. Shaded areas, simulations. The inset shows the Arnold tongue 1/2 on an enlarged scale. Note the splitting of the AT for higher modulation amplitudes and the excellent agreement between experiment and simulation.

(disregarding the dc offset) was normalized to 1, and the point in the parameter space where more than 25 Fourier peaks were found above the threshold $P_{th}=0.73$ was colored red. The fractal dimension was calculated at selected points in the red region, and the behavior was identified as chaotic. The green points represent values of ω_m and V_m where the response of the NMR laser was quasiperiodic. The blue points stand for (ω_m, V_m) values where the behavior of the laser was periodic, e.g., only higher harmonics of a single frequency were observed.

Figure 7(a) shows the results for the experiment, and Fig. 7(b) the corresponding calculations. The general trend is for the blue regions, which correspond to the locked states, to decrease in width with decreasing V_{m0} in accord with universal predictions for coupled oscillators [2]. In the experimental case the resolution (typically 20×20 grid points) was much lower than in the simulation (100×100 grid points). Correspondingly, the calculation shows features on a smaller scale than the experiment. Nevertheless the main features coincide. These include a

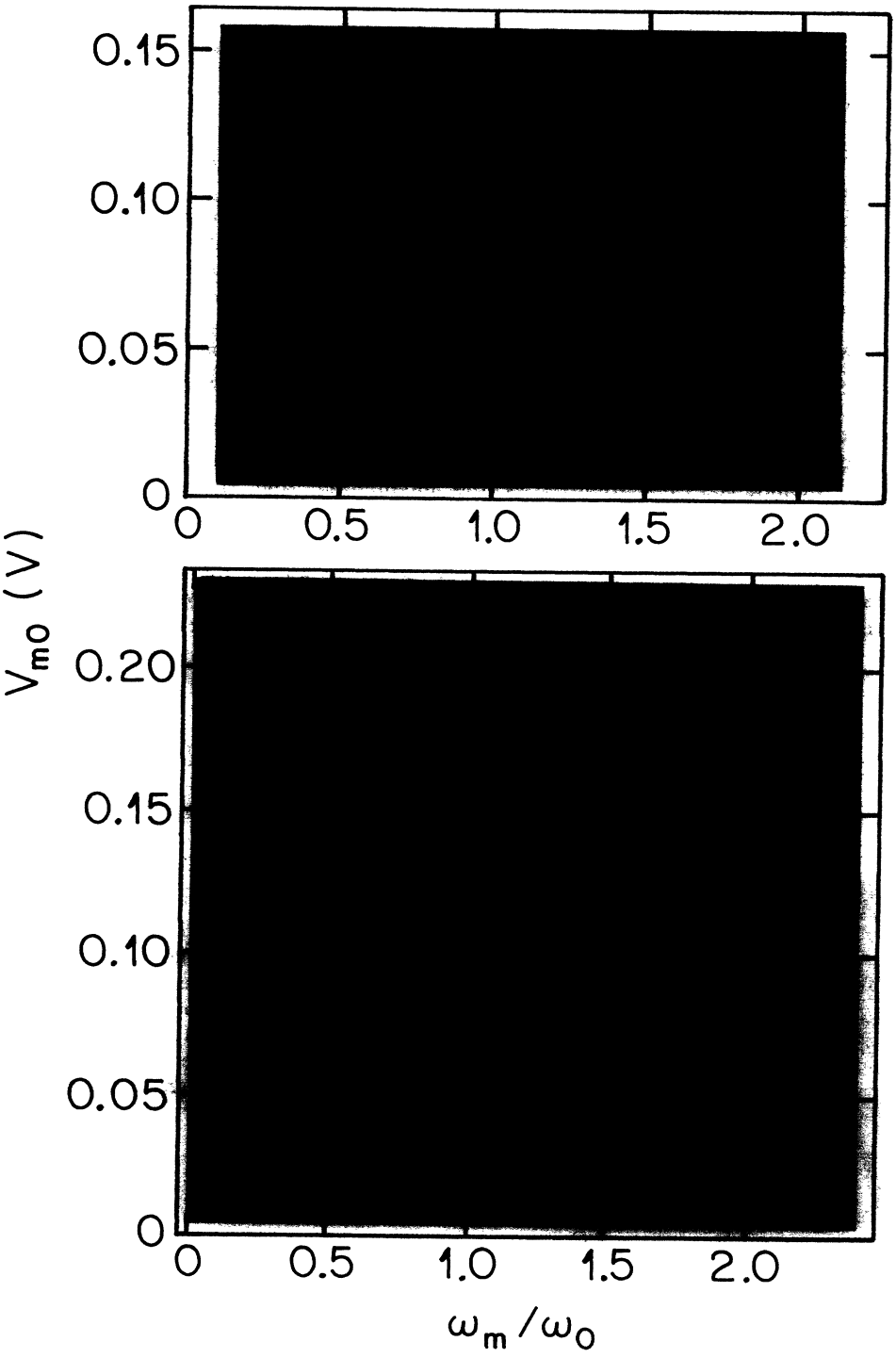

FIG. 7. Map of the type of dynamics in the parameter space of modulation frequencies vs modulation amplitude obtained by performing harmonic analysis on the time series; top, experiment and bottom, simulations. Blue points correspond to periodic time series, green to quasiperiodic, and red to chaotic time series. The main features agree very well, although the resolution was higher for the model calculations, resulting in more detailed structures.

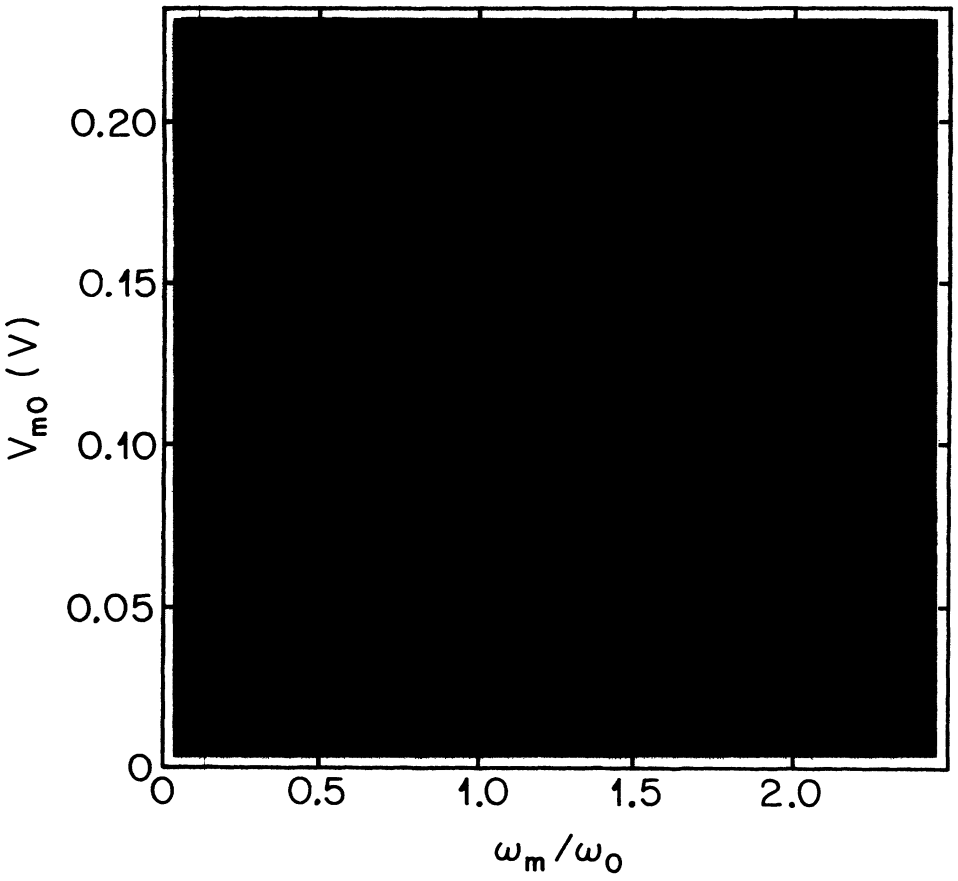

FIG. 8. Same as in Fig. 7 but for a reduced delay time of 41 ms.

splitting of the tongues for large modulation amplitudes (blue regions), and an insensitivity of the system to small modulation amplitudes (blue stripes at low modulation amplitudes). For comparison, Fig. 8 shows the results of the calculations for a delay time of 41 ms. The same transient time was used as in Fig. 7. Here the width of the Arnold tongue (AT) decreased in a monotonic way. Also, the quasiperiodic regimes (colored green) were more extended than for the $\tau=105$ ms delay time.

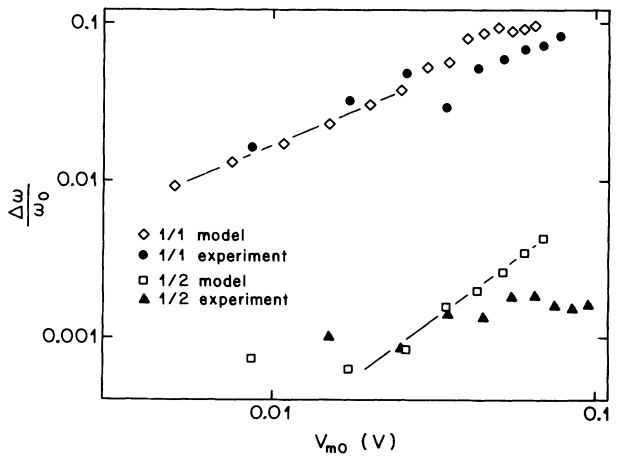

FIG. 9. Relative AT width vs modulation amplitude on a log-log scale showing the scaling behavior for the tongues 1/1 and 2/1 for the experiment and the model. The fitted exponents (straight lines) for the model are 0.85 for the 1/1 tongue and 1.6 for the 2/1 tongue.

The dependence of the width $\Delta\omega_m/\omega_0'$ on the modulation amplitude is shown in Fig. 9 for two selected AT's (1/2, 1/1) and a delay time of $\tau=105$ ms. Within a limited range of the modulation amplitude V_{m0}, a linear fit to the data suggested a power law scaling of the form

$$\Delta\omega(p/q) \propto V_{m0}^{b(p/q)} . \tag{12}$$

From the data one obtained $b(1/1)=0.85$ and $b(1/2)=1.6$.

V. ANHARMONIC MODULATION

In addition to the harmonic modulation discussed above, the influence of a square-wave modulation was studied. Two opposite effects were expected: on the one hand, since a square wave is composed of higher harmonics, part of which correspond to the limit cycle of the free-running system, the locking should be more effective; on the other hand, the abrupt changes of the modulation signal may drive the system into a chaotic regime for smaller amplitudes than in the case of a harmonic modulation. Both effects were indeed observed. The results are summarized in Fig. 10 both for the experiment and the simulations. Circles (squares) mark the boundary of locked states determined from experiment with the harmonic (anharmonic) modulation. The width of the locked states was significantly larger for the anharmonic modulation. In addition, the locking was more effective on the side of the Arnold tongue which exhibited smaller

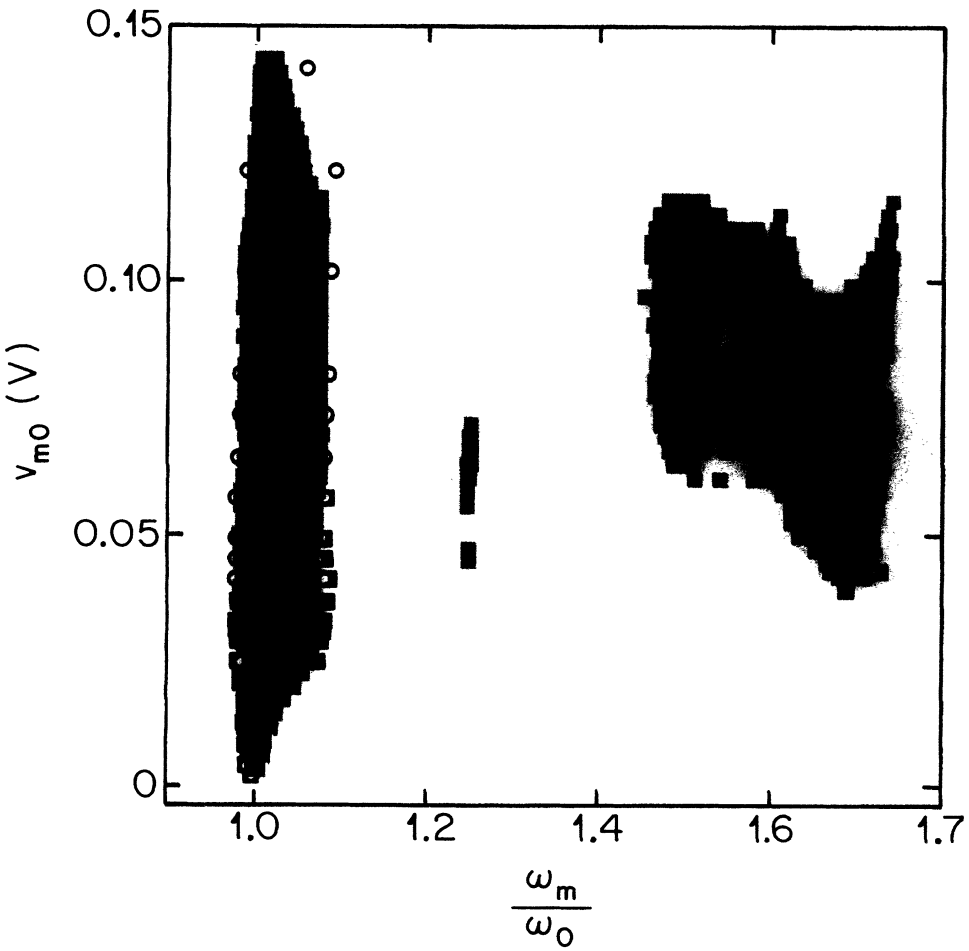

FIG. 10. Simulated and measured points showing locked states 1/1 and 2/1 with anharmonic (blue regions) and harmonic (green regions) modulations. The overlapping regions are colored red. The squares (anharmonic modulation) and circles (harmonic modulation) correspond to the measured border of the locked intervals. Note the significant broadening when modulated with an anharmonic signal, and also the rapid decay of the width of the AT in the case of anharmonic modulation with increased modulation amplitudes.

slopes. Also square-wave locking persisted only up to a certain value of V_{m0}, which was greatly reduced with respect to the value for the harmonic modulation. Both these effects were also found in the simulations. The green (blue) areas represent the locked states obtained from Eq. (11) for a harmonic (square-wave) modulation, and the red is the intersection of the two areas. The excellent agreement between experiment and model once again confirmed the validity of the EBL model.

VI. DISCUSSION

For a delay time of $\tau=105$ ms and harmonic modulation, the general behavior in some regimes (lower range of the modulation amplitude) was similar to those predicted by the circle map [2]. The width of the AT, within a limited range of modulation amplitude, followed the hierarchy described by the Farey tree, and the widths of the AT increased with modulation amplitude [2]. Significant deviations from the circle map included a nonmonotonic critical line which displayed a very complex dependence on modulation frequency. The rich structure of the critical line was probably due to the modulation, which caused the system to move periodically to the regime where two frequencies were present [Fig. 5(b)]. Thus one effectively has a system with three competing frequencies. Such systems have been shown to display very complex critical lines with extended AT boundaries, which consist of alternating chaotic, quasiperiodic, and periodic regimes [16]. The influence of the second frequency was evident for modulation amplitudes above $V_{m0}\approx 0.04$ V, where the AT's were split. In this case the system was locked to the limit cycle with fundamental frequency $\nu'_{00}\approx 34$ Hz. This is particularly obvious in tongues 1/1 and 2/1, as shown in Fig. 6. In this respect, the modulation of the quality factor can be seen as a sensitive method for forcing the different modes of the system to emerge, and stabilizing them.

Note also that locking was not observable near zero values in the modulation amplitude. In fact, the limit cycle was stable against the modulation up to some small threshold modulation amplitude.

VII. CONCLUSIONS

In conclusion, locked states were studied in the infinite-dimensional NMR laser with delayed feedback. With a delay time of $\tau=105$ ms the free-running system was evolving to an anharmonic limit cycle, whereas with a feedback delay of $\tau=41$ ms the system was quasiperiodic. In both cases, locking was observed by adding a periodic modulation to the feedback signal. The width of the AT's were significantly larger with an anharmonic square-wave modulation for small modulation amplitudes. For large modulation amplitudes the width of the AT rapidly decayed to zero for the square-wave modula-

tion, but continued to increase for the sinusoidal modulation. Furthermore, the AT broke up into distinct regimes of locking to limit cycles of different fundamental frequencies. All the experimental observations were modeled extremely well by the Bloch-Kirchhoff model with heuristic relaxation.

ACKNOWLEDGMENTS

The authors gratefully acknowledge many helpful discussions with R. Badii. This work was supported by the Swiss National Science Foundation and the Paul-Scherrer Institut.

[1] M. J. Higgins, A. A. Middleton, and S. Bhattacharya, Phys. Rev. Lett. **70**, 3784 (1993).
[2] M. H. Jensen, P. Bak, and T. Bohr, Phys. Rev. A **30**, 1960 (1984).
[3] M. Warden and F. Waldner, J. Appl. Phys. **64**, 5386 (1988).
[4] S. Martin and W. Martienssen, Phys. Rev. Lett. **56**, 1522 (1986).
[5] E. Brun, B. Derighetti, D. Meier, R. Holzner, and M. Ravani, J. Opt. Soc. Am. B **2**, 156 (1985).
[6] E. Brun, B. Derighetti, M. Ravani, G. Broggi, P. Meier, and R. Stoop, in *Proceedings of the Fourth International Symposium on Quantum Optics, Hamilton, New Zealand, 1986,* edited by J. D. Harwey and D. F. Walls, Springer Proceedings in Physics Vol. 12 (Springer-Verlag, Berlin, 1986), p. 119.
[7] L. Flepp, R. Holzner, E. Brun, M. Finardi, and R. Badii, Phys. Rev. Lett. **67**, 2244 (1991).
[8] For a recent review, see R. Badii, E. Brun, M. Finardi, L. Flepp, R. Holzner, J. Parisi, C. Reyl, and J. Simonet, Rev. Mod. Phys. (to be published).
[9] R. Holzner, L. Flepp, R. Stoop, G. Broggi, and E. Brun, Helv. Phys. Acta **62**, 910 (1989).
[10] See, e.g., A. N. Oraevsky, Kuant. Elektron. (Moscow) **19**, 979 (1992) [Sov. J. Quantum Electron. **22**, 910 (1992)]; F. T. Arecchi, G. Giacomelli, A. Lapucci, and R. Meucci, Phys. Rev. A **45**, R4225 (1992), and references therein; R. Lang and K. Kobayashi, IEEE J. Quantum Electron. **QE-16**, 347 (1980).
[11] A. Abragam, *Principles of Nuclear Magnetism* (Oxford University Press, Oxford, 1989).
[12] G. L. Oppo and A. Politi, Europhys. Lett. **1**, 11 (1986).
[13] R. Badii and A. Politi, Phys. Rev. Lett. **52**, 1661 (1984).
[14] G. Broggi, J. Opt. Soc. Am. B **5**, 1020 (1988).
[15] J. Mallet-Paret, J. Diff. Eq. **22**, 331 (1976).
[16] A. Cumming and P. S. Linsay, Phys. Rev. Lett. **60**, 2719 (1988).

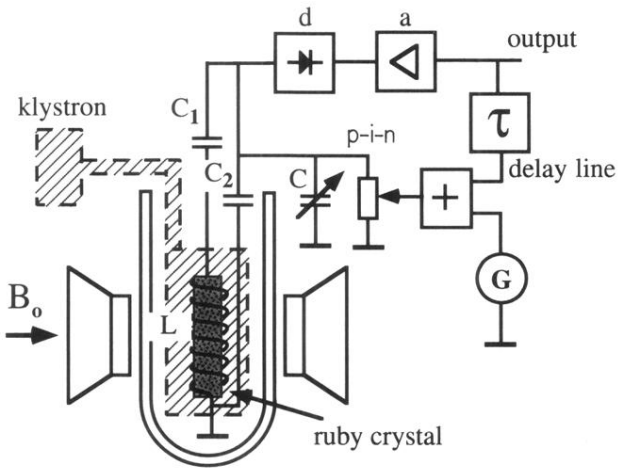

FIG. 1. Schematic representation of the experimental setup for the ruby NMR laser with delayed feedback and quality factor modulation. The gain medium consisted of the nuclear spins of the ^{27}Al nuclei within a ruby crystal which was subjected to a static field B_0. Population inversion was obtained by dynamic nuclear polarization with microwaves supplied by a klystron. The resonator was composed of a coil, a capacitive voltage splitter (C_1,C_2) and a tuning capacitor C, and a variable resistor (*p-i-n* diode). The laser output was fed back to the *p-i-n* diode after a delay time τ. In order to observe locking phenomena, periodic voltage modulation (G) was applied to the *p-i-n* diode.

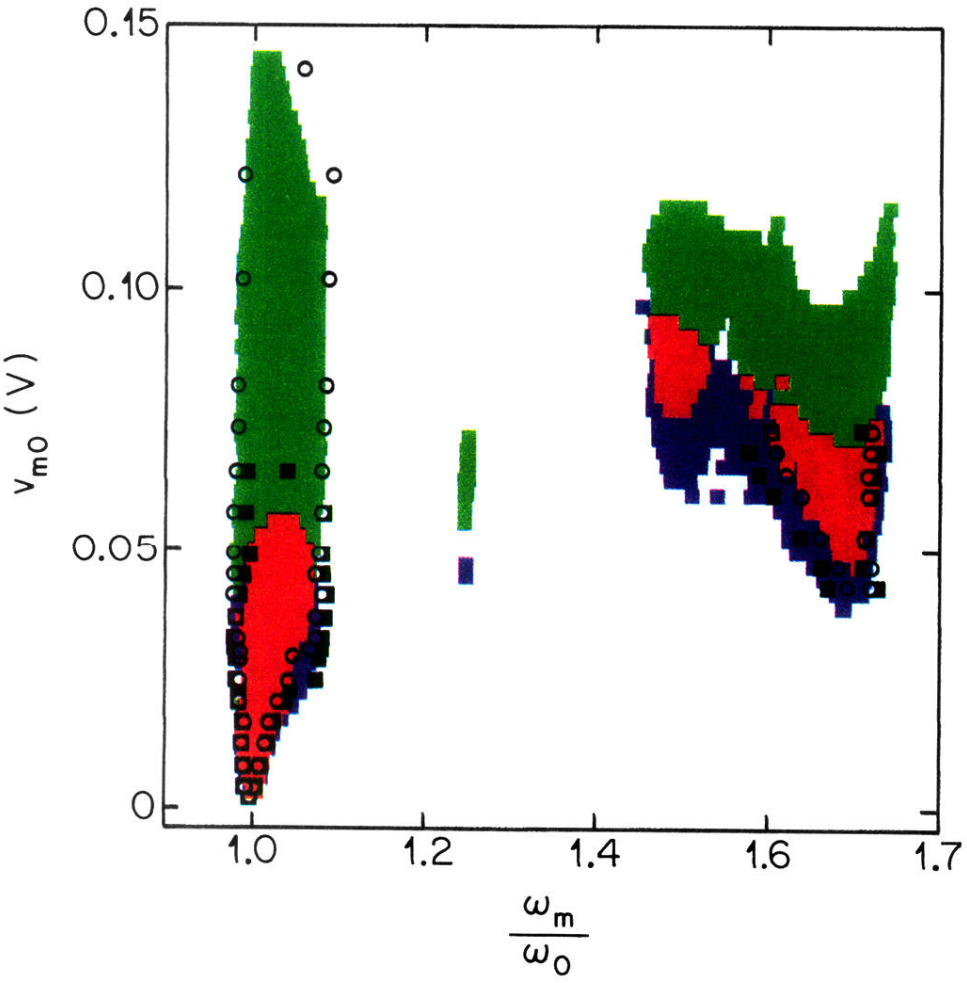

FIG. 10. Simulated and measured points showing locked states 1/1 and 2/1 with anharmonic (blue regions) and harmonic (green regions) modulations. The overlapping regions are colored red. The squares (anharmonic modulation) and circles (harmonic modulation) correspond to the measured border of the locked intervals. Note the significant broadening when modulated with an anharmonic signal, and also the rapid decay of the width of the AT in the case of anharmonic modulation with increased modulation amplitudes.

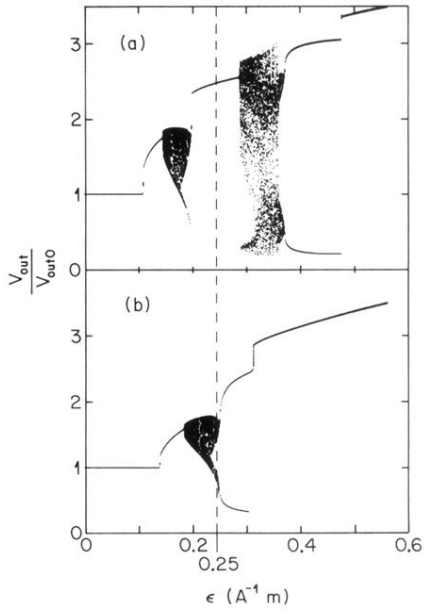

FIG. 2. Numerically determined bifurcation diagrams. For each feedback value ϵ the first 50 maxima were plotted after a transient time of 5 s. (a) $\tau = 105$ ms, (b) $\tau = 41$ ms. The dashed line corresponds to the ϵ value of the limit cycle used in subsequent studies of locking phenomena.

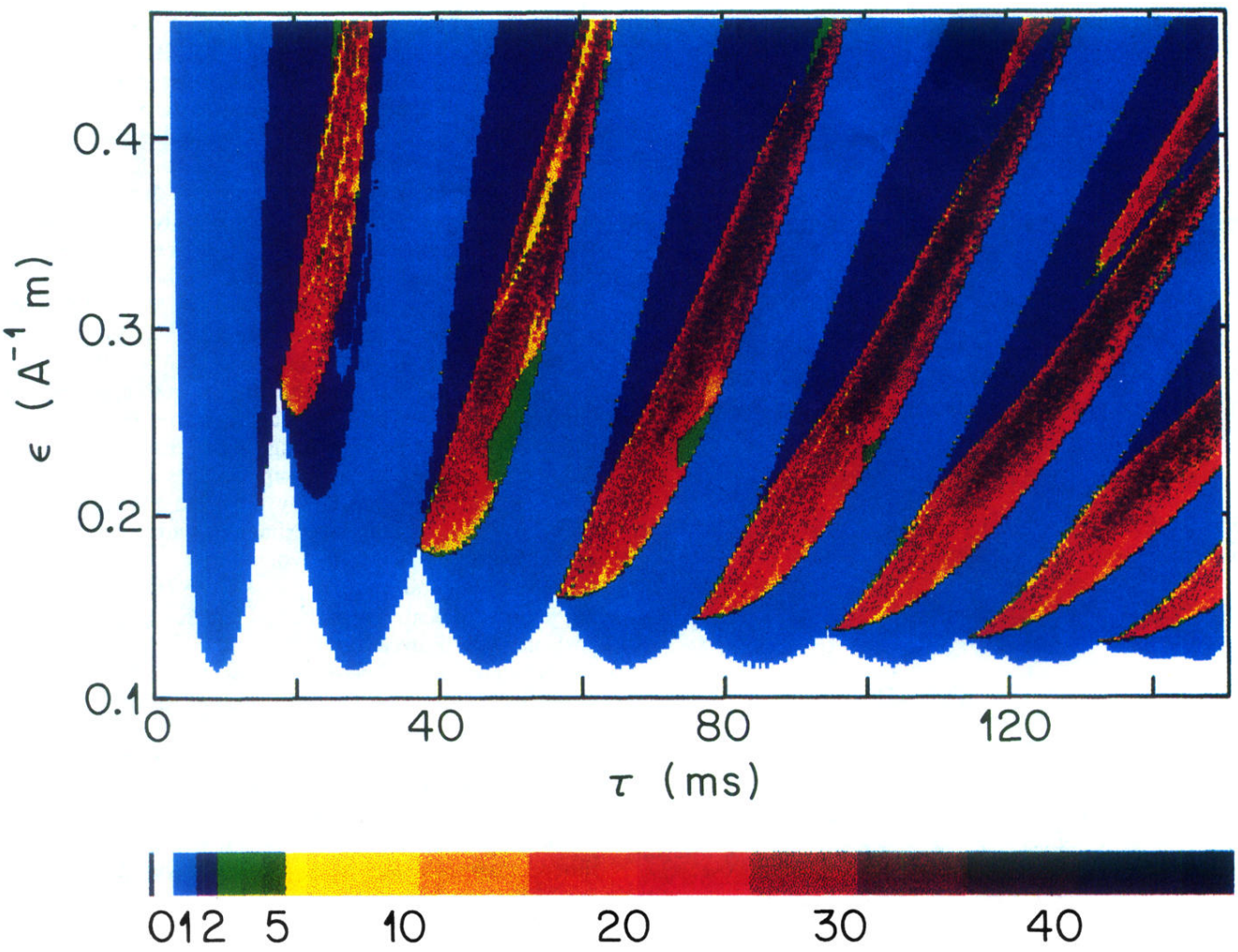

FIG. 3. Computed asymptotic properties of the solutions of the EBL model in the parameter space of delay time τ vs feedback coupling ϵ. The color coding corresponds to the number of maxima of different values in a time series of given length. White, stationary solutions. Light blue, period-2 solutions. Bottom, index showing the color used for a particular number of different maxima.

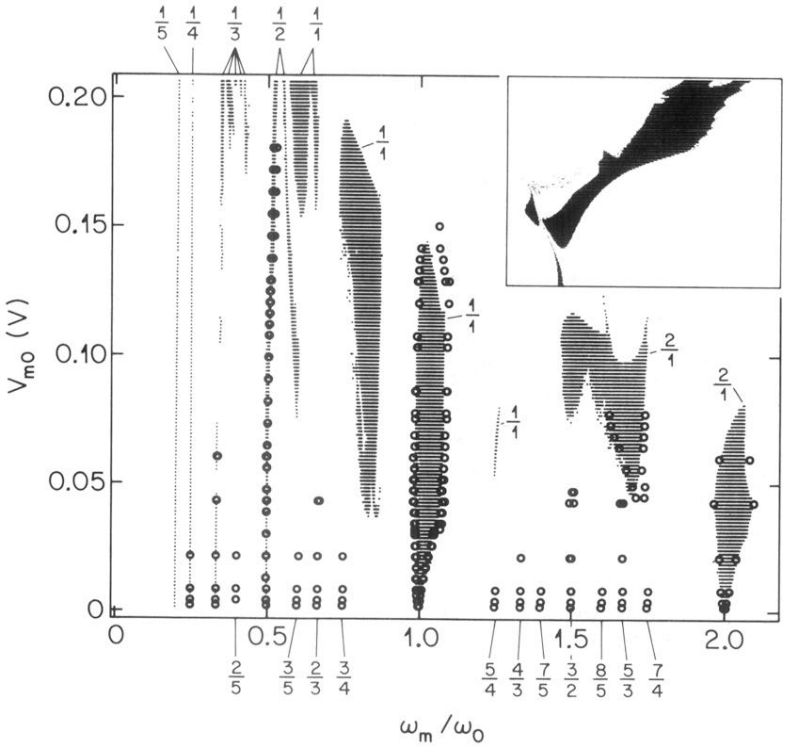

FIG. 6. Locked states in the parameter space of modulation frequency vs modulation amplitude. Circles, experiment. Shaded areas, simulations. The inset shows the Arnold tongue 1/2 on an enlarged scale. Note the splitting of the AT for higher modulation amplitudes and the excellent agreement between experiment and simulation.

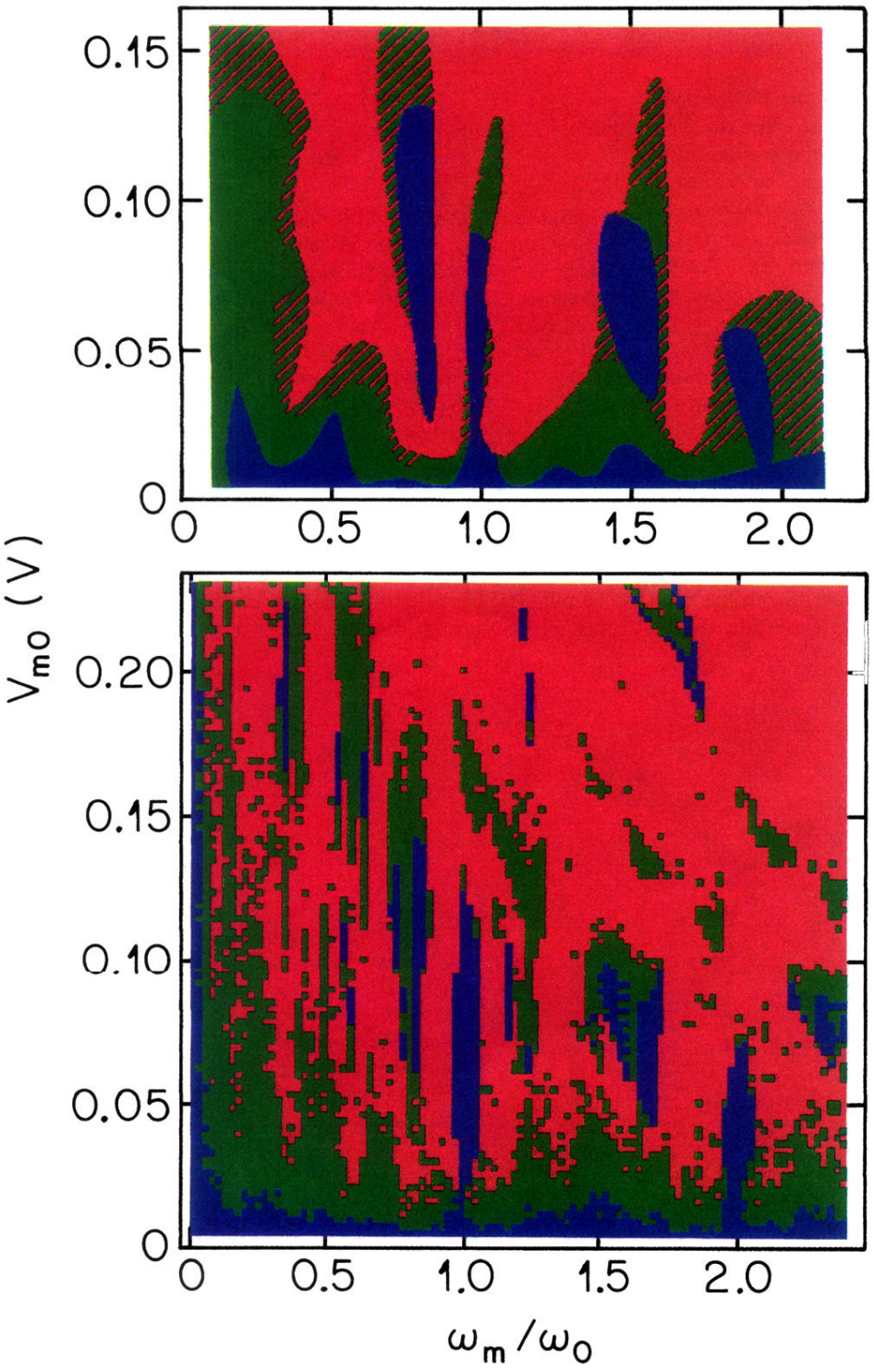

FIG. 7. Map of the type of dynamics in the parameter space of modulation frequencies vs modulation amplitude obtained by performing harmonic analysis on the time series; top, experiment and bottom, simulations. Blue points correspond to periodic time series, green to quasiperiodic, and red to chaotic time series. The main features agree very well, although the resolution was higher for the model calculations, resulting in more detailed structures.

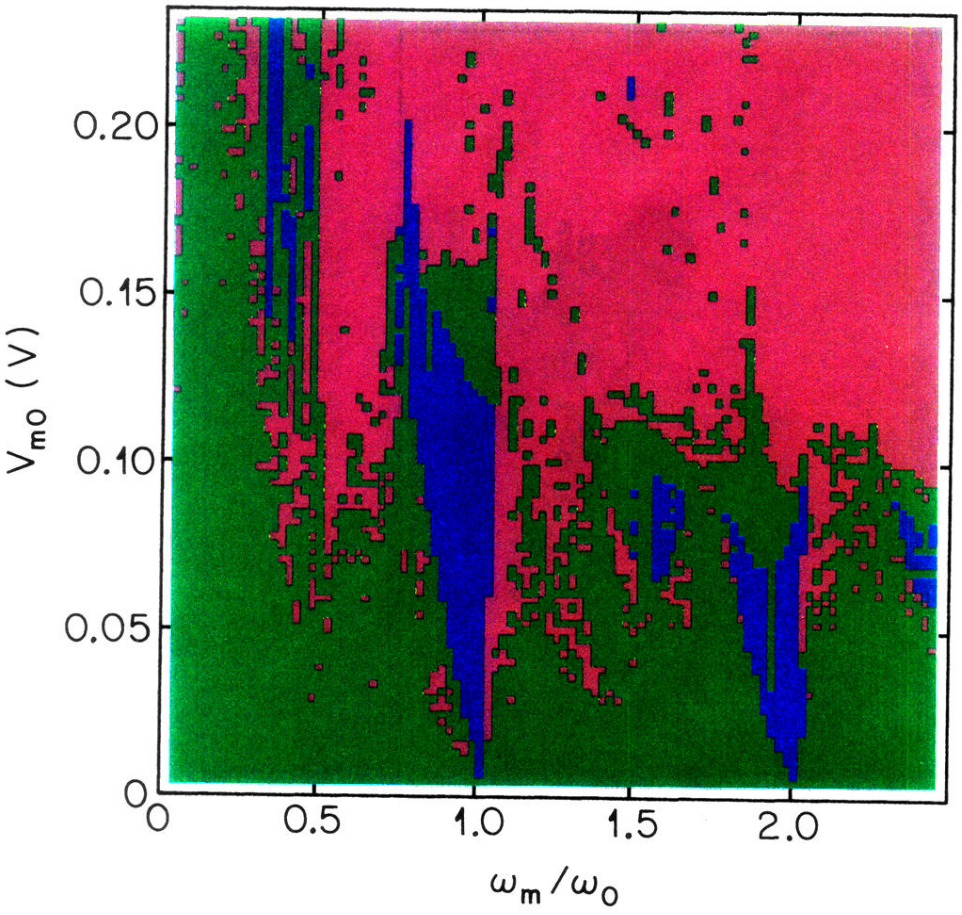

FIG. 8. Same as in Fig. 7 but for a reduced delay time of 41 ms.